International Journal of Architectural, Civil and Construction Sciences
ISSN: 2415-1734
Vol:12, No:11, 2018

Bidirectional Pendulum Vibration Absorbers with Homogeneous Variable Tangential Friction: Modelling and Design

Emiliano Matta

***Abstract*—**Passive resonant vibration absorbers are among the most widely used dynamic control systems in civil engineering. They typically consist in a single-degree-of-freedom mechanical appendage of the main structure, tuned to one structural target mode through frequency and damping optimization. One classical scheme is the pendulum absorber, whose mass is constrained to move along a curved trajectory and is damped by viscous dashpots. Even though the principle is well known, the search for improved arrangements is still under way. In recent years this investigation inspired a type of bidirectional pendulum absorber (BPA), consisting of a mass constrained to move along an optimal three-dimensional (3D) concave surface. For such a BPA, the surface principal curvatures are designed to ensure a bidirectional tuning of the absorber to both principal modes of the main structure, while damping is produced either by horizontal viscous dashpots or by vertical friction dashpots, connecting the BPA to the main structure. In this paper, a variant of BPA is proposed, where damping originates from the variable tangential friction force which develops between the pendulum mass and the 3D surface as a result of a spatially-varying friction coefficient pattern. Namely, a friction coefficient is proposed that varies along the pendulum surface in proportion to the modulus of the 3D surface gradient. With such an assumption, the dissipative model of the absorber can be proven to be nonlinear homogeneous in the small displacement domain. The resulting homogeneous BPA (HBPA) has a fundamental advantage over conventional friction-type absorbers, because its equivalent damping ratio results independent on the amplitude of oscillations, and therefore its optimal performance does not depend on the excitation level. On the other hand, the HBPA is more compact than viscously damped BPAs because it does not need the installation of dampers. This paper presents the analytical model of the HBPA and an optimal methodology for its design. Numerical simulations of single- and multi-story building structures under wind and earthquake loads are presented to compare the HBPA with classical viscously damped BPAs. It is shown that the HBPA is a promising alternative to existing BPA types and that homogeneous tangential friction is an effective means to realize systems provided with amplitude-independent damping.

***Keywords*—**Amplitude-independent damping, Homogeneous friction, Pendulum nonlinear dynamics, Structural control, Vibration resonant absorbers.

I. Introduction

PASSIVE resonant vibration absorbers are widely used dynamic control systems in civil engineering. In current applications, they simply consist in single-degree-of-freedom (SDOF) appendages, tuned to the target mode of the main structure through frequency and damping optimization [1]. One classical scheme is the pendulum absorber (PA), that uses gravity to generate the required restoring force, and consists of a damped mass constrained to move along an arched trajectory. A PA can be designed either as a supported pendulum, sliding or rolling along a physical track, or as a hanging pendulum, suspended through ropes or bars. In recent years, supported PAs have particularly attracted the interest of the research community, because of their compactness, durability and geometric versatility. Classical examples of supported PAs include the ball pendulum [2], the rolling and sliding pendulums (with single or double concavity) [3] and the rocking pendulum.

Despite the several technological realizations reported in the literature and available in engineering practice, the research for novel configurations is still under way, recently resulting in a number of new arrangements, including the unbalanced rolling PA [4], the multiple-ball PA [5], and several types of track nonlinear energy sinks [6]. In recent years this investigation has also inspired the proposal of the so-called BPA, consisting of a mass moving along an optimal 3D concave surface, whose principal curvatures are designed to ensure a bidirectional tuning to both principal structural modes. The BPA has been proposed in two different variants, respectively belonging to the supported pendulum and to the hanging pendulum types. The first variant is the rolling-pendulum absorber proposed in [7]. Its 3D surface is realized as a double 3D rolling-pendulum bearing, consisting of two equal concavities sandwiching a rolling ball. Changing the shape of the two concavities and the ball radius provides any possible 3D surface. The second variant is the hanging-pendulum absorber proposed in [8]. Its 3D surface is obtained through a Y-shaped arrangement of the suspending cables. Changing the length of the cables provides any possible toroidal surface. In the first variant, energy dissipation is produced by horizontal viscous dampers, whereas in the second variant it is produced by a vertically aligned friction damper. In this latter case, the orthogonality between the friction damper and the 3D surface ensures an amplitude-independent equivalent damping, which eventually makes the two variants approximately equivalent in terms of control effectiveness.

In this paper, a further alternative of BPA is presented, in which damping originates from the variable tangential friction force which develops between the pendulum mass and the 3D surface, as a result of a spatially-varying friction coefficient

E. Matta is with the Department of Architecture and Design, Politecnico di Torino, Turin, Italy (e-mail: emiliano.matta@polito.it).

pattern. In particular, the friction coefficient is assumed to vary along the guiding surface proportionally to the modulus of the surface gradient. This provides the absorber with a dissipative model which is nonlinear homogeneous in the small displacement domain [9]. This HBPA proves superior to conventional friction-type ball absorbers (characterized by a constant friction coefficient, as in [2] and [5]), because its equivalent damping ratio results independent of the amplitude of oscillations, and therefore, its optimal performance does not depend on the excitation level. On the other hand, with respect to the abovementioned existing types of BPAs ([7] and [8]), the HBPA is more compact, because its dissipation mechanism is integral with the guiding surface and no damper needs to be installed. In the HBPA, friction can be provided either by rolling or by sliding, depending on the type of supported pendulum chosen. The friction coefficient can be spatially varied through changing the surface roughness or the material or thickness of the surface coating, either continuously (according to the optimum pattern) or discretely (according to its stepwise approximation).

This paper describes the analytical model of the HBPA and proposes an optimal methodology for its design. Simulations of single-story and multi-story building structures subjected to wind and seismic loads are reported to highlight the pros and cons of the HBPA with respect to existing viscously damped BPAs (VBPA). Results show that the HBPA is a promising alternative to conventional VBPAs, and that homogeneous tangential friction is a possible solution to conceive mechanical systems characterized by amplitude-independent damping.

II. Description and Modelling of the HBPA

A. Problem Setting

A BPA including both viscous damping and tangential friction is schematically shown in Fig. 1.

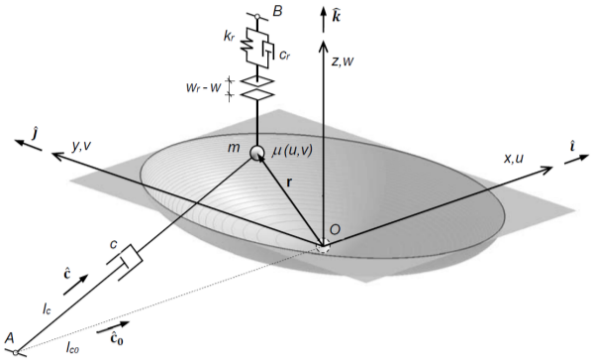

Fig. 1 Schematics of the BPA model

It is modelled as a point mass m subject to gravity g and constrained to move along a generic 3D surface, rigidly connected to the structure at its minimum in O. The motion of m along the surface is contrasted by: (i) the viscous damper connecting m to the structure in A; (ii) the friction force acting along the surface; and (iii) the restrainer (or bumper) connecting m to the structure in B. If the rotations of the structure are assumed negligible, the surface and the structural supports in A and B merely translate together with the support in O. If u, v and w are the coordinates of m with respect to the local reference system xyz fixed in O, and if $w = w(u,v) = w(\mathbf{q})$ is the pendulum surface equation, then the relative displacement of the HBPA with respect to the structure is $\mathbf{r} = [u,v,w]^T = [\mathbf{q}^T, w(\mathbf{q})]^T$, where u and v are the two independent coordinates, w is the dependent coordinate and $\mathbf{q} = [u,v]^T$ is the HBPA degree-of-freedom vector. The acceleration vector of the structural support is $\mathbf{a} = [a_x, a_y, a_z]^T = [\mathbf{a}_h^T, a_z]^T$, and the BPA relative velocity is derived as $\dot{\mathbf{r}} = (\partial \mathbf{r}/\partial \mathbf{q})\dot{\mathbf{q}} = \mathbf{J}\dot{\mathbf{q}}$, where $\mathbf{J} = \partial \mathbf{r}/\partial \mathbf{q} = [\mathbf{I}, \nabla w]^T$ is the Jacobian matrix of the kinematic transformation and $\nabla w = \partial w/\partial \mathbf{q}$ is the surface gradient.

B. The Dissipative Mechanisms

The model schematized in Fig. 3 accounts for three distinct dissipative mechanisms, respectively represented by: (i) one or more viscous dampers; (ii) the tangential friction mechanism; and (iii) the fail-safe restrainer.

Assuming for brevity a single viscous damper having damping coefficient c, undeformed length l_{c0}, deformed length l_c, and undeformed and deformed coaxial versors $\hat{\mathbf{c}}_0$ and $\hat{\mathbf{c}}$, and further denoting by $s_c = l_c - l_{c0}$ the damper axial elongation, it results that the viscous force vector acting on m is $\mathbf{f}_c = -f_c\hat{\mathbf{c}}$, where $f_c = c\dot{s}_c$ and $\dot{s}_c = \hat{\mathbf{c}}^T\dot{\mathbf{r}} = \hat{\mathbf{c}}^T\mathbf{J}\dot{\mathbf{q}}$.

Assuming a rigid-plastic (dry) friction coefficient varying along the pendulum surface according to an assigned geometrical pattern $\mu = \mu(u,v) = \mu(\mathbf{q})$, and denoting by N the modulus of the normal reaction force vector $\mathbf{N}$ at the contact point, the friction force vector acting on m can be expressed as $\mathbf{f}_\mu = -f_\mu\hat{\mathbf{t}}$, where $\hat{\mathbf{t}} = \dot{\mathbf{r}}/\|\dot{\mathbf{r}}\| = \mathbf{J}\dot{\mathbf{q}}/\sqrt{\dot{\mathbf{q}}^T\mathbf{J}^T\mathbf{J}\dot{\mathbf{q}}}$ is the tangent versor at the contact point and

$$f_\mu = \mu(\mathbf{q})N\,. \tag{1}$$

This paper focuses in particular on a special friction pattern, characterized by a friction coefficient proportional to the surface gradient vector according to:

$$\mu(\mathbf{q}) = \mu_0\|\nabla w\|\,, \tag{2}$$

where μ_0 is a properly selected proportionality factor, called the friction ratio. As it will be shown later, (2) ensures a homogeneous first-order friction model.

Assuming a restrainer having stiffness k_r, damping coefficient c_r and initial clearance w_r, the restrainer force vector acting on m is $\mathbf{f}_r = -f_r\hat{\mathbf{k}}$, where $f_r = 0$ if $w \le w_r$ and $f_r = k_r(w - w_r) + c_r\dot{w}$ if $w > w_r$, with $\dot{w} = \nabla w^T\dot{\mathbf{q}}$.

The total dissipative force applied to m by the three mechanisms is $\mathbf{f}_d = \mathbf{f}_c + \mathbf{f}_\mu + \mathbf{f}_r$. Denoting by $\mathbf{w} = -mg\hat{\mathbf{k}}$ the

weight of *m*, and by $\boldsymbol{\lambda}_d = m(\mathbf{a}+\ddot{\mathbf{r}})$ the dynamic interaction force exchanged between the BPA and its support, the dynamic equilibrium of *m* provides $\mathbf{w}+\mathbf{N}+\mathbf{f}_d = \boldsymbol{\lambda}_d$, which eventually allows to compute *N* in (1) as the modulus of the vector $\mathbf{N} = \boldsymbol{\lambda}_d - \mathbf{w} - \mathbf{f}_d$.

C.The Nonlinear 3D Model of the BPA

The dynamic equation of the BPA can be obtained by applying the Euler-Lagrange equation to the mass *m*:

$$\frac{d}{dt}\left(\frac{\partial T}{\partial \dot{\mathbf{q}}}\right) - \frac{\partial T}{\partial \mathbf{q}} + \frac{\partial V_g}{\partial \mathbf{q}} + \mathbf{Q}_i + \mathbf{Q}_e = \mathbf{0}, \tag{3}$$

where $T = m\dot{\mathbf{r}}^T\dot{\mathbf{r}}/2$ is the kinetic energy of *m*; V_g=*mgw* is its gravitational potential energy; $\mathbf{Q}_i = -\mathbf{J}^T\mathbf{f}_d$ is the generalized internal force due to the total dissipative force $\mathbf{f}_d$; and $\mathbf{Q}_e = m\mathbf{J}^T\mathbf{a}$ is the generalized external force due to the support acceleration. Deriving the first three terms of (3), and denoting by $\mathbf{M}^q = m\mathbf{J}^T\mathbf{J}$ the BPA generalized mass matrix, the fully nonlinear 3D model of the device can be finally obtained as follows:

$$\mathbf{M}^q\ddot{\mathbf{q}} + \mathbf{Q}_i + mg\nabla w = -m\mathbf{J}^T\mathbf{a} - \left(\dot{\mathbf{M}}^q\dot{\mathbf{q}} - \frac{\partial T}{\partial \mathbf{q}}\right). \tag{4}$$

In (4), the dissipative term on the left-hand side can be expressed as:

$$\mathbf{Q}_i = -\mathbf{J}^T\mathbf{f}_d = f_c\mathbf{J}^T\hat{\mathbf{c}} + f_\mu\mathbf{J}^T\hat{\mathbf{t}} + f_r\mathbf{J}^T\hat{\mathbf{k}}, \tag{5}$$

where

$$f_c\mathbf{J}^T\hat{\mathbf{c}} = c\left(\mathbf{J}^T\hat{\mathbf{c}}\hat{\mathbf{c}}^T\mathbf{J}\right)\dot{\mathbf{q}}, \tag{6}$$

$$f_\mu\mathbf{J}^T\hat{\mathbf{t}} = \mu(\mathbf{q})N\mathbf{J}^T\mathbf{J}\dot{\mathbf{q}}/\sqrt{\dot{\mathbf{q}}^T\mathbf{J}^T\mathbf{J}\dot{\mathbf{q}}}, \text{ and} \tag{7}$$

$$f_r\mathbf{J}^T\hat{\mathbf{k}} = f_r\nabla w \tag{8}$$

respectively, represent the generalized viscous, friction and restrainer force vectors.

D.The Nonlinear 3D Model of the BPA-MDOF System

The dynamic equation of a linear multi-degree-of-freedom (MDOF) structure subjected to external forces and ground accelerations and equipped with the BPA is:

$$\mathbf{M}_s\ddot{\mathbf{q}}_s + \mathbf{C}_s\dot{\mathbf{q}}_s + \mathbf{K}_s\mathbf{q}_s + \mathbf{L}^T\boldsymbol{\lambda}_d = \mathbf{f}_s - \mathbf{M}_s\mathbf{R}_s\ddot{\mathbf{r}}_g, \tag{9}$$

where $\mathbf{q}_s$ is the vector of structural DOFs; $\mathbf{M}_s$, $\mathbf{C}_s$ and $\mathbf{K}_s$ are the structural matrices of mass, damping and stiffness; $\mathbf{f}_s$ is the vector of external forces; $\ddot{\mathbf{r}}_g$ is the vector of ground accelerations; $\mathbf{L}$ and $\mathbf{R}_s$ are kinematic and topological matrices. By combining (4) and (9), the fully nonlinear dynamic equation of the coupled system can be finally expressed as:

$$\begin{bmatrix}\mathbf{M}_s + m\mathbf{L}^T\mathbf{L} & m\mathbf{L}^T\mathbf{J}\\ m\mathbf{J}^T\mathbf{L} & \mathbf{M}^q\end{bmatrix}\begin{bmatrix}\ddot{\mathbf{q}}_s\\ \ddot{\mathbf{q}}\end{bmatrix} + \begin{bmatrix}\mathbf{C}_s & \mathbf{0}\\ \mathbf{0} & \mathbf{0}\end{bmatrix}\begin{bmatrix}\dot{\mathbf{q}}_s\\ \dot{\mathbf{q}}\end{bmatrix} + \begin{bmatrix}\mathbf{K}_s & \mathbf{0}\\ \mathbf{0} & \mathbf{0}\end{bmatrix}\begin{bmatrix}\mathbf{q}_s\\ \mathbf{q}\end{bmatrix} + \\ + \begin{bmatrix}\mathbf{0}\\ \mathbf{Q}_i\end{bmatrix} = \begin{bmatrix}\mathbf{f}_s\\ \mathbf{0}\end{bmatrix} - \begin{bmatrix}\mathbf{M}_s + m\mathbf{L}^T\mathbf{L}\\ m\mathbf{J}^T\mathbf{L}\end{bmatrix}\mathbf{R}_s\ddot{\mathbf{r}}_g - \begin{bmatrix}m\mathbf{L}^T\dot{\mathbf{J}}\dot{\mathbf{q}}\\ \dot{\mathbf{M}}^q\dot{\mathbf{q}} - \dfrac{\partial T}{\partial \mathbf{q}}\end{bmatrix}. \tag{10}$$

E.The First-Order Approximated Model

Fundamental properties of the BPA can be highlighted by considering its response in the small-displacement domain. By developing in Taylor series expressions (4) to (8), and by truncating higher-order terms, the first-order 3D model of the BPA is obtained as

$$m\ddot{\mathbf{q}} + \mathbf{C}\dot{\mathbf{q}} + N_0\mathbf{K}_w\mathbf{q} + \mu_0 N_0\left\|\mathbf{K}_w\mathbf{q}\right\|\dot{\mathbf{q}}/\left\|\dot{\mathbf{q}}\right\| = -m\mathbf{a}_h, \tag{11}$$

where: **C** is the BPA viscous damping matrix, given by:

$$\mathbf{C} = c\begin{bmatrix}\hat{c}_{0x}^2 & \hat{c}_{0x}\hat{c}_{0y}\\ \hat{c}_{0x}\hat{c}_{0y} & \hat{c}_{0y}^2\end{bmatrix} \tag{12}$$

if the viscous damper is set parallel to the *xy* plane; $N_0 = N/(mg) = 1+a_z/g$ is the weight-normalized normal component of the reaction force vector; $\mathbf{a}_h = [a_x, a_y]^T$ is the vector of horizontal accelerations at the support; and $\mathbf{K}_w$ is the equivalent pendular stiffness matrix, given by:

$$\mathbf{K}_w = \begin{bmatrix}k_{wx} & 0\\ 0 & k_{wy}\end{bmatrix} = mg\begin{bmatrix}1/L_x & 0\\ 0 & 1/L_y\end{bmatrix} = mg\mathbf{H}_w, \tag{13}$$

where $\mathbf{H}_w$ is the Hessian matrix of $w(\mathbf{q})$ in $\mathbf{0}$, and L_x and L_y are the pendulum lengths in the local directions *x* and *y*.

Accordingly, the first-order 3D model of the BPA-structure coupled system is expressed as:

$$\begin{bmatrix}\mathbf{M}_s + m\mathbf{L}_h^T\mathbf{L}_h & m\mathbf{L}_h^T\\ m\mathbf{L}_h & m\mathbf{I}\end{bmatrix}\begin{bmatrix}\ddot{\mathbf{q}}_s\\ \ddot{\mathbf{q}}\end{bmatrix} + \begin{bmatrix}\mathbf{C}_s & \mathbf{0}\\ \mathbf{0} & \mathbf{C} + \mu_0 N_0\left\|\mathbf{K}_w\mathbf{q}\right\|/\left\|\dot{\mathbf{q}}\right\|\end{bmatrix}\begin{bmatrix}\dot{\mathbf{q}}_s\\ \dot{\mathbf{q}}\end{bmatrix} + \\ + \begin{bmatrix}\mathbf{K}_s & \mathbf{0}\\ \mathbf{0} & N_0\mathbf{K}_w\end{bmatrix}\begin{bmatrix}\mathbf{q}_s\\ \mathbf{q}\end{bmatrix} = \begin{bmatrix}\mathbf{f}_s\\ \mathbf{0}\end{bmatrix} - \begin{bmatrix}\mathbf{M}_s + m\mathbf{L}_h^T\mathbf{L}_h\\ m\mathbf{L}_h\end{bmatrix}\mathbf{R}_s\ddot{\mathbf{r}}_g, \tag{14}$$

where $\mathbf{L}_h$ is the vector containing the first two columns of **L**.

Based on (11) it can be observed that:

1) the inertia force vector $m\ddot{\mathbf{q}}$ and the restoring force vector $N_0\mathbf{K}_w\mathbf{q}$ are linear and uncoupled along *x* and *y*; this holds for the viscous force vector $\mathbf{C}\dot{\mathbf{q}}$, provided that all viscous dampers are aligned with the coordinate axes;
2) the friction force vector has modulus $\mu_0 N_0\left\|\mathbf{K}_w\mathbf{q}\right\|$ and has direction and sign of the tangent versor $\dot{\mathbf{q}}/\left\|\dot{\mathbf{q}}\right\|$; because its

modulus, direction and sign are nonlinear and coupled, the friction force vector is a nonlinear coupled function of $\mathbf{q}$ and $\dot{\mathbf{q}}$;

3) because its modulus increases proportionally with $\mathbf{q}$ and does not depend on $\dot{\mathbf{q}}$, the friction force vector is a homogeneous function of $\mathbf{q}$ and $\dot{\mathbf{q}}$; (11) itself is therefore homogeneous and its solution is proportional to the horizontal acceleration $\mathbf{a}_h$, which definitely makes an HBPA a first-order nonlinear but homogeneous system.

F.The Simplified 2D Model

The 3D first-order models in (11) and (14) can be further simplified for design purposes by assuming that: (i) the motion occurs in a vertical coordinate plane, supposedly the *xz* plane, so the models turn into 2D models; (ii) in the *xz* plane the structural target frequency is far from the other ones, so the MDOF structure can be reduced to a 1DOF mode-generalized system; (iii) the vertical acceleration input a_z is negligible, so $N_0 = 1$. Under these conditions, (11) and (14), respectively, become:

$$m\ddot{u} + c_x\dot{u} + k_{wx}[1+\mu_0\text{sign}(u\dot{u})]u = -ma_x, \tag{15}$$

$$\begin{bmatrix} m_{sx}+m & m \\ m & m \end{bmatrix}\begin{bmatrix} \ddot{u}_s \\ \ddot{u} \end{bmatrix} + \begin{bmatrix} c_{sx} & 0 \\ 0 & c_x \end{bmatrix}\begin{bmatrix} \dot{u}_s \\ \dot{u} \end{bmatrix} + \\ + \begin{bmatrix} k_{sx} & 0 \\ 0 & k_{wx}[1+\mu_0\text{sign}(u\dot{u})] \end{bmatrix}\begin{bmatrix} u_s \\ u \end{bmatrix} = \begin{bmatrix} f_{sx} \\ 0 \end{bmatrix} - \begin{bmatrix} m_{sx}+m \\ m \end{bmatrix}\ddot{u}_g, \tag{16}$$

where u_s is the structure horizontal displacement relative to the ground; m_{sx}, c_{sx} and k_{sx} are the structure generalized mass, damping and stiffness along *x*; and c_x is the BPA viscous damping coefficient along *x*.

Equations (15) and (16) can be finally recast in modal form as follows:

$$\ddot{u} + 2\varsigma_x\omega_x\dot{u} + \omega_x^2[1+\mu_0\text{sign}(u\dot{u})]u = -a_x, \tag{17}$$

$$\begin{bmatrix} 1+m_{Rx} & m_{Rx} \\ 1 & 1 \end{bmatrix}\begin{bmatrix} \ddot{u}_s \\ \ddot{u} \end{bmatrix} + 2\omega_{sx}\begin{bmatrix} \varsigma_{sx} & 0 \\ 0 & \varsigma_x\omega_{Rx} \end{bmatrix}\begin{bmatrix} \dot{u}_s \\ \dot{u} \end{bmatrix} + \\ + \omega_{sx}^2\begin{bmatrix} 1 & 0 \\ 0 & \omega_{Rx}^2[1+\mu_0\text{sign}(u\dot{u})] \end{bmatrix}\begin{bmatrix} u_s \\ u \end{bmatrix} = \begin{bmatrix} \bar{f}_{sx} \\ 0 \end{bmatrix} - \begin{bmatrix} 1+m_{Rx} \\ 1 \end{bmatrix}\ddot{u}_g, \tag{18}$$

where $m_{Rx} = m/m_{sx}$ is the BPA mass ratio along *x*; $\omega_{sx} = \sqrt{k_{sx}/m_s}$ and $\omega_x = \sqrt{g/L_x}$ are the structure and BPA circular frequencies along *x*; $\omega_{Rx} = \omega_x/\omega_{sx}$ is the BPA frequency ratio along *x*; and $\varsigma_{sx} = c_{sx}/(2\omega_{sx}m_{sx})$ and $\varsigma_x = c_x/(2\omega_x m)$ are the structure and BPA viscous damping ratios along *x*.

III. Design Methodology

A design methodology is here proposed for a BPA of either viscous type (VBPA) or homogeneous variable friction type (HBPA). Their respective models can be obtained from those derived in Section II, by respectively annulling the friction or the viscous terms. The methodology comprises two steps: (1) a 2D first-order optimization; and (2) a 3D second-order completion.

A.The 2D First-Order Optimization Step

Based on the simplified 2D model expressed by (18), which admits an uncoupled motion along *x* and *y*, and assuming the structure known, both the VBPA and the HBPA are completely defined, in each direction, by three dimensionless design parameters, namely m_{Rx}, ω_{Rx} and ς_x for the VBPA, and m_{Rx}, ω_{Rx} and μ_0 for the HBPA. If, as usual in vibration absorbers design, the mass ratio m_{Rx} is fixed based on cost-benefit expectations, the two remaining free parameters can be determined by solving a classical H_∞ design problem [10], i.e. by minimizing the H_∞ norm of some meaningful input-output transfer function of the structure-BPA system. Denoting by ω the circular frequency of the excitation input, two possible transfer functions are here considered for each BPA type, namely the force-to-displacement transfer function $T_f(\omega)$ (computed from $\bar{f}_{sx}$ to u_s and significant for wind load applications) and the ground acceleration-to-displacement transfer function $T_g(\omega)$ (computed from $\ddot{u}_g$ to u_s and significant for seismic load applications). Denoting as the response ratio R_x the ratio between the controlled and the uncontrolled H_∞ norm of those transfer functions, optimization can be formalized as follows, respectively for a wind-oriented VBPA:

$$R_{xopt} = \min_{\omega_{Rx},\varsigma_x} R_x = \min_{\omega_{Rx},\varsigma_x}\max_{\omega}\left(\left|T_f(\omega)\right|^{con} \Big/ \left\|T_f\right\|_\infty^{unc}\right), \tag{19}$$

for a seismic-oriented VBPA:

$$R_{xopt} = \min_{\omega_{Rx},\varsigma_x} R_x = \min_{\omega_{Rx},\varsigma_x}\max_{\omega}\left(\left|T_g(\omega)\right|^{con} \Big/ \left\|T_g\right\|_\infty^{unc}\right), \tag{20}$$

for a wind-oriented HBPA:

$$R_{xopt} = \min_{\omega_{Rx},\mu_0} R_x = \min_{\omega_{Rx},\mu_0}\max_{\omega}\left(\left|T_f(\omega)\right|^{con} \Big/ \left\|T_f\right\|_\infty^{unc}\right), \tag{21}$$

and for a seismic-oriented HBPA:

$$R_{xopt} = \min_{\omega_{Rx},\mu_0} R_x = \min_{\omega_{Rx},\mu_0}\max_{\omega}\left(\left|T_g(\omega)\right|^{con} \Big/ \left\|T_g\right\|_\infty^{unc}\right). \tag{22}$$

Equations (19) and (20) provide the optimal VBPA parameters ω_{Rxopt} and ς_{xopt}, respectively for wind and seismic control. Equations (21) and (22) provide the optimal HBPA parameters ω_{Rxopt} and μ_{0opt}, respectively for wind and seismic control.

The min.max. problems (19)-(22) are numerically solved by using a branch & bound search algorithm similar to the one used in [3], followed by a nonlinear least-square solver that improves local convergence. The computation of the VBPA

transfer function in (19) and (20) is straightforward and based on classical closed-form expressions available for linear mechanical models, whereas the computation of the HBPA transfer function in (21) and (22) requires simulating the response time-history of the system at each input frequency until the response amplitude stabilizes at an acceptable degree.

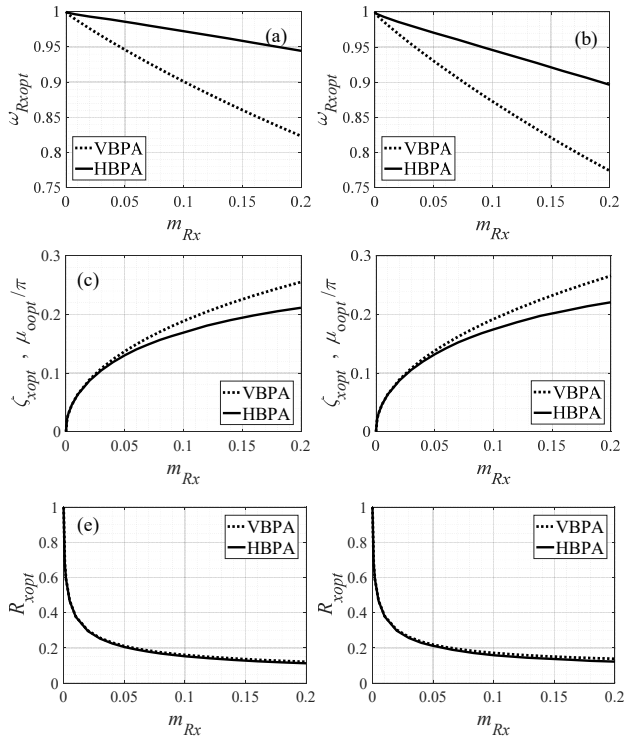

Fig. 2 H_∞ optimal design of a VBPA (dotted lines) and a HBPA (continuous lines), for ζ_{sx} = 2% and as a function of m_{Rx}. On the left: wind-oriented design. On the right: seismic-oriented design. First row: optimal frequency ratios. Second row: optimal viscous/friction damping ratios. Third row: optimal response ratios

Assuming a structural damping ratio ζ_{sx} = 2%, the results of the optimization are shown in Fig. 2 for both the VBPA (dashed lines) and the HBPA (continuous lines), as a function of the mass ratio m_{Rx} (ranging from 1‰ to 20%). The wind-oriented optimization is reported on the left (subfigures a, c and e), while the seismic-oriented optimization is reported on the right (subfigures b, d and f). The first row of subfigures (a and b) shows the optimal frequency ratio; the second row (c and d) shows the optimal damping ratio (for the VBPA) and the optimal friction ratio (for the HBPA), this latter conveniently normalized to π; and the third row (e and f) shows the resulting optimal response ratios. Whereas the results obtained for the VBPA are well known (see for instance [11]) and do not deserve specific comments, the results obtained for the HBPA interestingly reveal that the optimal HBPA generally (although not largely) improves the VBPA performance (resulting in a smaller response ratio), especially for large values of m_{Rx}. To achieve this, ω_{Rxopt} is always larger for the HBPA than for the VBPA, except for very small mass ratios, when the optimal frequency ratio converges to unity for both types. On the other hand, μ_{0opt} appears to converge to $\pi \cdot \varsigma_{xopt}$ for small mass ratios, but to be increasingly smaller than $\pi \cdot \varsigma_{xopt}$ as the mass ratio increases. The same trends are observed for both the wind-oriented and the seismic-oriented design types.

Assuming, as it will be done in the sequel, that the target modes of the structure have the same damping ratio and the same generalized mass in the two horizontal directions, the results obtained above identically hold along x and y, and the x subscript can be dropped for brevity in the expressions for the parameters and the response ratios. Together with the mass ratio m_R and with the structural parameters, the resulting optimal dimensionless parameters ω_{Ropt}, ς_{opt} and μ_{0opt} provide then all the BPA dimensional parameters involved in the domain of the small displacement, i.e. the BPA mass m, the BPA circular frequencies ω_x and ω_y, the BPA pendulum lengths L_x and L_y, the VBPA damping coefficients c_x and c_y, and the HBPA friction pattern around the origin, this latter given around the origin by:

$$\mu(\mathbf{q}) = \mu_{0opt} \left\| \nabla w \right\| \approx \mu_{0opt} \sqrt{u^2 / L_x^2 + v^2 / L_y^2} \,. \tag{23}$$

B. The 3D Second-Order Completion Step

The completion step provides the BPA parameters which, involved only in the large-displacement domain, are excluded from the optimization step. They include the shape of the pendulum surface (and consequently the friction pattern) far from the origin, the length and number of the viscous dampers and the properties of the restrainer. These parameters could undergo a specific optimization process based on the fully nonlinear model, but for simplicity they are here left to the free choice of the designer. Some guidelines for their selection are proposed as follow.

By providing L_x and L_y, the optimization step completely determines the pendulum shape around the origin. Far from it, however, different shapes correspond to the same pair of L_x and L_y. Among the viable choices are, for example, the ellipsoid, the torus or the elliptic paraboloid. If the ellipsoid is chosen, as in the sequel, infinite ways of assigning its semi-axes b_x, b_y and b_z exist which provide the desired L_x and L_y pair. However, by imposing that $b_z = \sqrt{b_x b_y}$ only one admissible ellipsoid exists, of semi-axes $b_x = \sqrt[4]{L_x^3 L_y}$, $b_y = \sqrt[4]{L_x L_y^3}$ and $b_z = \sqrt{L_x L_y}$. This choice will be assumed in the remaining of this paper.

With the said assumption of an ellipsoidal pendulum shape, the friction pattern defined by (2) specializes as:

$$\mu(\mathbf{q}) = \mu_{0opt} \sqrt{\left(\frac{u^2}{L_x^2} + \frac{v^2}{L_y^2} \right) \Big/ \left(1 - \frac{u^2}{b_x^2} - \frac{v^2}{b_y^2} \right)}, \tag{24}$$

where $\mu(\mathbf{q})$ tends to zero around the origin, tends to infinite at the ellipsoid equator, and describes iso-friction curves

(characterized by a constant friction value) which intersect the level curves (characterized by a constant height), as shown for example in Fig. 3, which refers to an ellipsoid having L_y/L_x = 2, and truncated at $w_r = b_z/2$. Both Figs. 3 (a) and (b) represent nine level curves, uniformly spaced from 0 to w_r, and nine iso-friction curves, uniformly spaced from 0 to 2 μ_{0opt}.

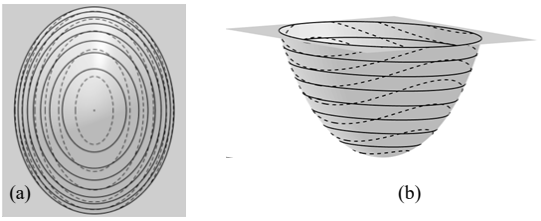

Fig. 3 Level curves (continuous) and iso-friction curves (dashed) if L_y/L_x = 2: (a) planar view; (b) axonometric view (with the z dimension doubled for clarity)

Regarding the design of the viscous dampers, the optimization step provides the optimal values of c_x and c_y, based on the assumption of a single damper in each direction. If more dampers are used in the same direction, the optimal damping coefficient must be parted among them. The length of the viscous dampers does not enter the optimization step. In the sequel, two dampers will be assumed in every direction, each having length $l_{c0} = b_z = \sqrt{L_x L_y}$.

Finally, the restrainer too does not enter the optimization step. Its mechanical properties shall be assigned to simulate a dissipative impact. In the remaining of this paper, its stiffness is assigned as $k_r = m\omega_r^2$, where $\omega_r = 20\sqrt{\omega_x \omega_y}$; its damping is assigned as $c_r = 2\varsigma_r \omega_r m$, where $\varsigma_r = -\ln e_r \Big/ \sqrt{\pi^2 + \ln^2 e_r}$ and e_r = 0.5 (elastic restitution coefficient); its clearance is assigned as $w_r = b_z/2$.

IV. 2D Simulations of the First-Order Model

This section compares the optimal VBPA and the optimal HBPA in the small-displacement domain, by assuming the first-order 2D models expressed by (16) or (18). The structure is a 2% damped SDOF system.

A. White noise force input

Optimized according to the wind-oriented design method exposed in Section III, the VBPA and the HBPA are here compared by subjecting the SDOF structure to a stationary Gaussian zero-mean white-noise normalized force input $\bar{f}_{sx}$. For the uncontrolled and for the VBPA-controlled structure (linear cases), the stationary root-mean-square (rms) response of the system is computed by solving the Lyapunov equation [10]. For the HBPA-controlled structure (homogeneous nonlinear case), the rms response is computed by Monte Carlo simulations, using 100 realizations of the input process. Each realization has a duration of $3600T_{sx}$ and a sampling time of $0.01T_{sx}$, T_{sx} being the structural period.

The BPA performance is here evaluated in terms of the rms structural displacement, rms(u_s), and the rms BPA relative displacement (stroke), rms(u). In particular, two performance indices are considered, obtained dividing the controlled value of these rms responses by the uncontrolled value of the rms structural displacement: the displacement response ratios R_{dx} = rms$(u_s)_{con}$/ rms$(u_s)_{unc}$, and the stroke response ratio R_{sx} = rms$(u)_{con}$/ rms$(u_s)_{unc}$.

The two response ratios are reported in Fig. 4, where they appear nearly identical for the two BPA types. The substantial equivalence already observed under a harmonic force input in Fig. 2 (e) is therefore confirmed under a white-noise force input. Expectedly, the absorber results more effective in H_∞ terms than against a white-noise input (i.e. in H_2 terms).

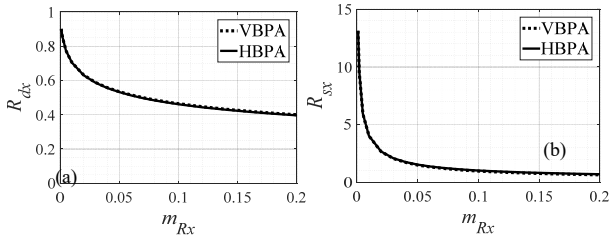

Fig. 4 2D first-order model. VBPA and HBPA response ratios under a unidirectional white-noise force input

B. Real Seismic Ground Acceleration Input

Optimized according to the seismic-oriented design method, the evaluation of the VBPA and the HBPA under a white-noise ground acceleration input $\ddot{u}_g$ leads to very similar results to those presented in Fig. 4, which are therefore omitted here for brevity.

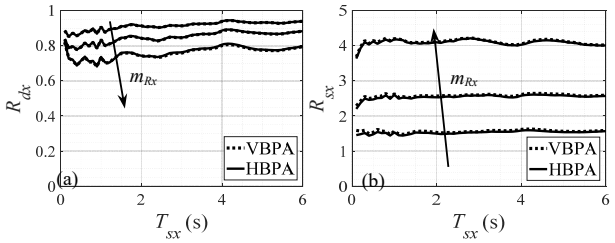

Fig. 5 2D first-order model. VBPA and HBPA response ratio spectra under a unidirectional seismic input, for m_{Rx} = 1%, 3%, 10%

More interestingly, the structure (with or without BPA) is here subjected to a set of 338 near-field real seismic records (details in [12]), and its period T_{sx} is varied from 0.1 s to 6.0 s so as to obtain uncontrolled and controlled spectra. For each response quantity of interest, namely the maximum structural displacement $u_{s,max}$ and the maximum BPA stroke u_{max}, the 338 spectra are then condensed into their rms spectrum. Dividing, at each period, the controlled rms response spectra by the uncontrolled structural displacement response spectrum, two significant rms response ratio spectra are obtained, respectively in terms of structural displacement (R_{dx} = rms$(u_{s,max})_{con}$/ rms$(u_{s,max})_{unc}$) and in terms of BPA stroke (R_{sx} = rms$(u_{max})_{con}$/ rms$(u_{s,max})_{unc}$). Results are reported in Fig. 5 for

three mass ratios (m_{Rx} = 1%, 3% and 10%). Again, the VBPA and the HBPA display a very alike performance, both in terms of structural displacement and absorber strokes.

V. 3D Simulations of the First-Order Model

This section extends the analysis to 3D models, still operating in the small-displacement domain, according to (14). The equations of motion are still linear and uncoupled for the VBPA but nonlinear and coupled for the HBPA. The structure is a 2%-damped system having 1 DOF in each direction.

A. White Noise Force Input

The structure, having T_{sx} = 1 s and T_{sy}/T_{sx} variable from 1 (axial-symmetry) to 2, is supposed to be excited by two independent white-noise force input components f_{sx} and f_{sy}, having the same rms value $f_{sx0} = f_{sy0}$. The mass ratio $m_R = m_{Rx} = m_{Ry}$ is supposed to alternatively equal 1%, 3% and 10%. The BPA performance is evaluated by considering the average response to 100 realizations of the stochastic input process, each one having duration 600 s and sampling time 0.01 s. Performance is expressed by the following two bidirectional response ratios: $R_d = \sqrt{R_{dx}R_{dy}}$ and $R_s = \sqrt{R_{sx}R_{sy}}$, which extend to 3D the 2D response ratios already introduced in Section IV.A.

Results are reported in Fig. 6, where R_d and R_s are plotted as a function of T_{sy}/T_{sx}. The VBPA performance appears clearly constant with T_{sy}/T_{sx}. The HBPA performance appears approximately constant with T_{sy}/T_{sx}, and quite similar to the VBPA performance, with only slightly larger structural displacements and moderately smaller BPA strokes.

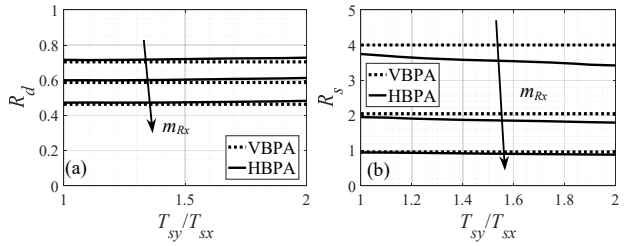

Fig. 6 3D first-order model under a bidirectional white-noise force input. VBPA and HBPA response ratios as a function of T_{sy}/T_{sx}, for m_{Rx} = 1%, 3%, 10%

B. Real Seismic Ground Acceleration Input

The bidirectional performance of the VBPA and of the HBPA is here evaluated using the same set of seismic records adopted in Section IV.B. Spectra are expressed in terms of 3D rms response ratios, obtained by averaging the corresponding 2D rms response ratios in the x and y directions, according to: $R_d = \sqrt{R_{dx}R_{dy}}$ and $R_s = \sqrt{R_{sx}R_{sy}}$. Fig. 7 shows R_d and R_s computed under the assumption that T_{sy}/T_{sx} = 1, for $T_{sx} = T_{sy}$ ranging from 0.5 to 4.0 s, and for m_R alternatively equal to 1%, 3% or 10%. As already recognized in Fig. 6, it appears that under bidirectional excitation, because of friction coupling, the nearly perfect coincidence between the VBPA and the HBPA response is lost. Friction damping implies a slightly larger structural response, and a slightly smaller stroke. The extent of this reduction remains however quite limited.

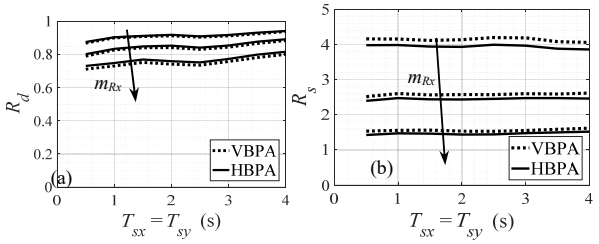

Fig. 7 3D first-order model. VBPA and HBPA response ratio spectra under a bidirectional seismic input, for T_{sy}/T_{sx} = 1 and m_{Rx} = 1%, 3%, 10%

VI. 2D Simulations of the Fully Nonlinear Model

In order to show the influence of the excitation intensity on the BPA performance, this section compares the optimal VBPA and the optimal HBPA in the large-displacement domain, by assuming fully nonlinear 2D models. The structure is once again a 2% damped SDOF system.

A. White Noise Force Input

A structure controlled with a wind-optimal BPA having m_{Rx} = 3% is simulated under a unidirectional white-noise force input of rms amplitude $\bar{f}_{sx0}$, duration 600 s and sampling time 0.01 s. The response ratios R_{dx} and R_{sx} are reported in Fig. 8 for the two types of BPA as a function of $\bar{f}_{sx0}$ ranging from 0 to 5 N/kg.

For $\bar{f}_{sx0}$ = 0, the results are those already obtained in Fig. 4 for first-order models. As $\bar{f}_{sx0}$ increases, the structural displacement mitigation effectiveness diminishes, as typical of pendulum devices, and the absorber stroke decreases, as a result of bumping on the restrainer and loss of tuning. The effectiveness reduction appears delayed for the HBPA with respect to the VBPA, because of the amplitude-increasing dissipation capabilities of the gradient-proportional friction pattern, instead of the amplitude-decreasing equivalent damping ensured by the viscous dashpots under large displacements.

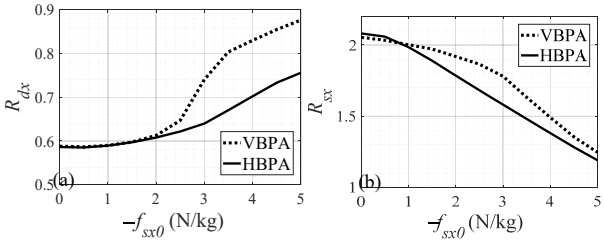

Fig. 8 2D fully nonlinear model. VBPA and HBPA response ratios under a unidirectional white-noise force input, as a function of the input level and for m_{Rx} = 3%

B.Real Seismic Ground Acceleration Input

A structure controlled with a seismic-optimal BPA having m_{Rx} = 3% is simulated under the set of real records already introduced in Section IV.B, for increasing seismic intensities. Denoting by I the intensity ratio, i.e. the dimensionless factor adopted to scale the entire set of records, Fig. 9 reports R_{dx} and R_{sx} as a function of I, for the two BPA types and for two possible periods of the structure, namely T_{sx} = 0.5 s (top subfigures) and T_{sx} = 4.0 s (bottom subfigures).

For I = 0, the results are those already obtained in Fig. 5 for first-order models. As I increases, both R_{dx} and R_{sx} decrease for both structural periods, as already observed in Section VI.A under force excitation. However, significant variations are solely observed for T_{sx} = 0.5 s, as a result of the limited stroke capacity of small-period pendulums. In this case, the HBPA appears again superior to the VBPA, by virtue of the increasing damping provided by the proposed friction pattern.

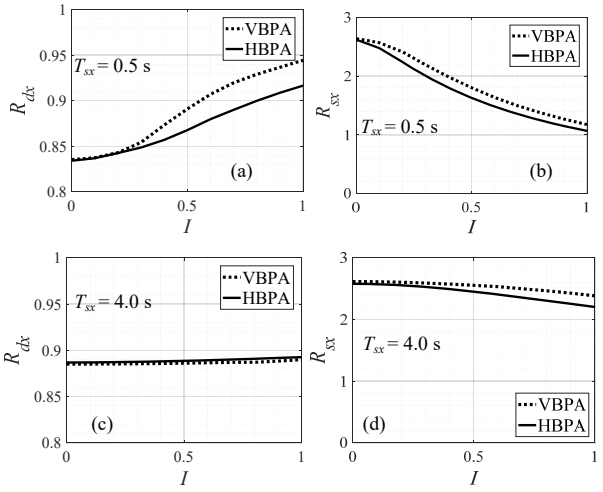

Fig. 9 2D fully nonlinear model. VBPA and HBPA response ratio spectra under a unidirectional seismic input, as a function of I and for m_{Rx} = 3%. Top figures: T_{sx} = 0.5 s; bottom figures: T_{sx} = 4.0 s

VII. 3D Simulations of the Fully Nonlinear Model

This section generalizes the previous results to a 3D model.

A.White Noise Force Input

The optimal BPAs are supposed to be mounted on a 2%-damped structure having 1 DOF in each direction, with T_{sx} = T_{sy} = 1 s. The structure is excited by a bidirectional white-noise force input, having equal rms amplitude in the two directions $\bar{f}_{sx0} = \bar{f}_{sy0}$, duration 600 s and sampling time 0.01 s. Simulations are conducted for $\bar{f}_{sx0} = \bar{f}_{sy0}$ ranging from 0 to 5 N/kg, and results are reported in Fig. 10. The performance loss trends already observed for a unidirectional input in Fig. 8 are confirmed. Again, the HBPA performance is similar to the VBPA performance for small intensities, and better for large ones.

B.Real Seismic Ground Acceleration Input

Table I reports the response ratios obtained by subjecting the controlled structure to the bidirectional seismic records included in the selected set, for m_R = 3% and for the intensity ratio increasing from 0 to 0.5 to 1.0. Two cases are considered, with the first structural period T_{sx} being fixed at 1.0 s and the second structural period T_{sy} equaling either 1.0 s or 1.5 s. Table I confirms that under a bidirectional shaking the VBPA is preferable if second-order effects are negligible (I = 0), and the HBPA if they are not.

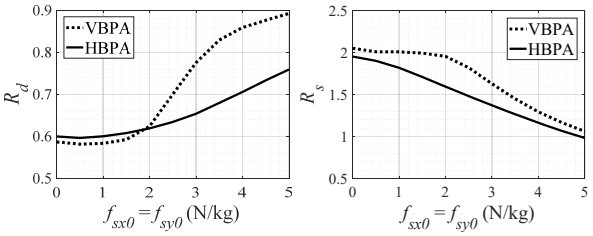

Fig. 10 3D fully nonlinear model. VBPA and HBPA response ratios under a bidirectional white-noise force input, as a function of the input level and for m_{Rx} = 3%. T_{sx} = T_{sy} = 1.0 s

TABLE I
3D Fully Nonlinear Model under Seismic Input. RMS Response Ratios for Different Periods and Intensities (m_R = 3%)

		R_d		R_s	
	I	VBPA	HBPA	VBPA	HBPA
T_{sx} = 1.0 s, T_{sy} = 1.0 s	0.0	0.83	0.84	2.60	2.47
	0.5	0.90	0.88	1.81	1.52
	1.0	0.95	0.92	1.16	1.00
T_{sx} = 1.0 s, T_{sy} = 1.5 s	0.0	0.84	0.85	2.58	2.35
	0.5	0.88	0.87	2.00	1.64
	1.0	0.94	0.91	1.38	1.15

VIII. An MDOF Building under Wind Load

An MDOF high-rise building structure exposed to wind loads is simulated in this section with or without a BPA atop, by using the fully nonlinear model expressed by (10). The BPA is either of the VBPA or of the HBPA type, and in both cases is optimized according to the wind-oriented design procedure exposed in Section III.

The structure is 168 m tall with a 25 m x 25 m square section. Its shape, mass and stiffness are taken from [13], but scaled to augment the building sensitivity to the across-wind component. Modelled as a tapered 10-elements cantilever beam, the structure has a flexural stiffness which in the y direction is 1.21 times smaller than in the x direction. The natural periods along y are therefore 1.10 times larger than along x. In the x direction, the first three periods are 4.00 s, 1.23 s, and 0.52 s, with participating modal masses of 45.3%, 21.8%, and 11.1%. Damping is assumed as 2% in every mode.

The BPA mass is assumed as 1% the total building mass, corresponding to an effective mass ratio of 6.45% according to Warburton's approach [1]. By applying the design methodology presented in Section III, the VBPA and the HBPA parameters are computed as in Table II.

Simulations are performed under moderate-to-high wind flow, blowing for 1 hour either along x or along y. Deterministic wind load time-histories are determined as the realization of a stationary, spatially nonhomogeneous, stochastic process, comprising both along-wind and across-wind components, therefore exciting the structure simultaneously in the two directions. Along- and across-wind components are computed based on classical wind load spectra [14], [15].

TABLE II
BPA DESIGN PARAMETERS ON THE TALL BUILDING

	ω_R (-)	ς (-)	μ_0 (-)	L_x (m)	L_y (m)	b_x (m)	b_y (m)	b_z (m)	l_{c0} (m)	w_r (m)
VBPA	0.93	0.15	-	4.57	5.53	4.79	5.27	5.03	5.03	2.51
HBPA	0.98	-	0.45	4.12	4.99	4.32	4.76	4.53	-	2.27

For brevity, results are presented in Table III only for the wind blowing in the x direction. Four cases are compared, corresponding respectively to: (1) the uncontrolled structure; (2) the ideally linear VBPA; (3) the (geometrically nonlinear) VBPA; and (4) the HBPA. For each case, several response quantities are reported, including: (i) the maximum modulus of the top story displacement, $r_{N,max}$; (ii) the maximum modulus of the BPA stroke, r_{max}; (iii) the maximum friction damping ratio encountered by the HBPA along the surface, μ_{max}; (iv) the rms of the modulus of the top story displacement, $r_{N,rms}$; (v) the rms of the modulus of the BPA stroke, r_{rms}; and the mean value of the instantaneous power dissipated by the structure, $W_{s,mean}$.

TABLE III
BUILDING RESPONSES FOR WIND BLOWING ALONG X

Case	$r_{N,max}$ (cm)	r_{max} (cm)	μ_{max} (-)	$r_{N,rms}$ (cm)	r_{rms} (cm)	$W_{s,mean}$ (kW)
Uncontrolled	79.4	0.0	-	27.3	0.0	31.1
Linear VBPA	39.6	110	-	13.7	37.5	8.12
VBPA	39.7	109	-	13.8	37.4	8.17
HBPA	38.4	107	0.10	13.7	37.8	8.63

Table III shows that:

1) With respect to the uncontrolled structure, the ideally linear VBPA achieves a significant response reduction, with a 50% reduction in $r_{N,max}$ and in $r_{N,rms}$, and with a 74% reduction in $W_{s,mean}$.
2) The VBPA, modelled accounting for geometrical nonlinearities, gives nearly identical results to the ideally linear VBPA. The absorber strokes are relatively small and the restrainer is far from being activated, which makes the first-order model accurate enough.
3) The HBPA performance is also very similar to the VBPA performance. The greatest differences are in $W_{s,mean}$, which is 6% larger for the HBPA, and in $r_{N,max}$, which is 3% larger for the VBPA. The maximum friction coefficient met by the HBPA during motion is 0.10.

It can be concluded that the three controlled cases are substantially equivalent.

IX. CONCLUSION

The following main conclusions can be drawn:

1) The HBPA proves roughly equivalent to the VBPA, particularly when responding to a unidirectional excitation in the small displacement domain.
2) Both types suffer a performance loss if the stroke demand exceeds their stroke capacity, which usually occurs in rigid structures under large input intensities. This drawback is partially attenuated for the HBPA because of its larger dissipation capacity at large displacements. Despite such loss, in all considered cases both types still provide a significant control action.

REFERENCES

[1] G. B. Warburton, "Optimum absorber parameters for various combinations of response and excitation parameters," *Earth. Eng. Struct. Dyn*., vol. 10, pp. 381–401, 1982.
[2] J. Náprstek, C. Fischer, M. Pirner, and O. Fischer, "Non-linear model of a ball vibration absorber," *Comput. Meth. Applied Sciences*, vol. 30, pp. 381–396, 2013.
[3] E. Matta, and A. De Stefano, "Robust design of mass-uncertain rolling pendulum TMDs for the seismic protection of buildings," *Mech. Syst. Sign. Proc.*, vol. 23, pp. 127–147, 2009.
[4] M. Bransch, "Unbalanced oil filled sphere as rolling pendulum on a flat surface to damp horizontal structural vibrations," *J. Sound Vibr.*, vol. 368, pp. 22–35, 2016.
[5] J. Chen, and C. T. Georgakis, "Tuned rolling-ball dampers for vibration control in wind turbines," *J. Sound Vibr.*, vol. 332, pp. 5271–5282, 2013.
[6] J. Wang, N. E. Wierschem, B. F. Spencer Jr, and X. Lu, "Track nonlinear energy sink for rapid response reduction in building structures," *J. Eng. Mech.*, vol. 141, no. 1, pp. 1–10, 2015.
[7] E. Matta, A. De Stefano, and B. F. Spencer Jr, "A new passive rolling-pendulum vibration absorber using a non-axial-symmetrical guide to achieve bidirectional tuning," *Earthq. Eng. Struct. Dyn.*, vol. 38, pp. 1729–1750, 2009.
[8] J. L. Almazan, J. C. De la Llera, J. A. Inaudi, D. Lopez-Garcia, and L. E. Izquierdo. "A Bidirectional and homogeneous tuned mass damper: a new device for passive control of vibrations," *Eng. Struct.*, vol. 29, pp. 1548–1560, 2007.
[9] J. Inaudi, and J. Kelly, "Mass damper using friction-dissipating devices," *J. Eng. Mech*., vol. 121, pp. 142–149, 1995.
[10] J. B. Burl, *Linear Optimal Control*. Menlo Park, CA: Addison-Wesley, Longman, 1999.
[11] A. Y. T. Leung, and H. Zhang, "Particle swarm optimization of tuned mass dampers," *Eng. Struct.*, vol. 31, pp. 715–728, 2009.
[12] E. Matta, "Effectiveness of Tuned Mass Dampers against Ground Motion Pulses," *J. Struct. Eng.*, vol. 139, no. 2, pp. 188–198, 2013.
[13] Y. L. Xu, B. Samali, and K. C. S. Kwok, "Control of along-wind response of structures by mass and liquid dampers," *J. Eng. Mech.*, vol. 118, no. 1, pp. 20–39, 1992.
[14] A. G. Davenport, "The spectrum of horizontal gustiness near the ground in high winds," *Q. J. R. Meteorol. Soc.*, vol. 87, pp. 194–211, 1961.
[15] B. J. Vickery, and A. W. Clarke, "Lift or across-wind response of tapered stacks," *J. Struct. Div. ASCE*, vol. 98, pp. 1–20, 1972.